Proceedings of IMECE2006
2006 ASME International Mechanical Engineering Congress and Exposition
November 5-10, 2006, Chicago, Illinois, USA

IMECE2006-14151

CONTROL OF A PEM FUEL CELL COOLING SYSTEM

Richard T. Meyer* **and Bin Yao**
Systems, Measurement, and Control
School of Mechanical Engineering
Purdue University
West Lafayette, IN 47907-1288
Email: rtmeyer@purdue.edu

ABSTRACT

Previous research has assumed that a perfect Proton Exchange Membrane Fuel Cell (PEMFC) body temperature manager is available. Maintaining this temperature at a desired value can ensure a high reaction efficiency over all operation. However, fuel cell internal body temperature control has not been specifically presented so far. This work presents such control, using a Multiple Input Single Output (MISO) fuel cell cooling system to regulate the internal body temperature of a PEMFC intended for transportation. The cooling system plant is taken from a recently developed hydrogen/air PEMFC total system model. It is linearized and used to design a series of controllers via μ-synthesis. μ-synthesis is chosen since system nonlinearities can be handled as parameter uncertainties. A controller must coordinate the desired fuel cell internal temperature and commanded mass flow rates of the coolant and cooling air. Each linear controller is created for a segment of the expected current density range. Plant parameters are expected to vary over their linearized values in each segment. Also, a common set of μ-synthesis weighting functions has been developed to ease controller design at different operating points. Thus, the nonlinear cooling subsystem can be controlled with a series of current density scheduled linear controllers. Current density step change simulations are presented to compare the controller closed loop performance and open loop response which uses cooling system flow rates taken from an optimal steady state solution of the whole fuel cell system. Furthermore, a closed loop sinusoid response is also given. These show that the closed loop driven internal fuel cell temperature will vary little during operation. However, this will only be true over the range that the cooling system is required to be active.

NOMENCLATURE

c_v	Average specific heat at constant volume (J/kg K)
CV	Control volume
d	Exogenous input
e	Error
f_S	Factor of safety
m	Mass (kg)
P	Plant
T	Temperature (K)
u	Control input
W	Weighting function
x	State vector
y	System output
δ	Difference, $\delta a = a - a_o$, a a variable
Δ	Deviation
μ	Structured singular value
ω	Rotational speed (rad/s)

Subscripts

act	Actuator
bw	Bandwidth
cds	Current density segment
clt	Coolant
$dist$	Disturbance

*Address all correspondence to this author.

fan Cooling fan
fc Fuel cell
ha Humidified air
hex Heat exchanger
max Maximum
min Minimum
mu Multiplicative uncertainty
o Operating point
$perf$ Performance
$snois$ Sensor noise
unc Uncertain

INTRODUCTION

The PEMFC is a device that produces electrical power via oxidation and reduction half reactions that are separated in space. In this case, the fuel is hydrogen gas and the oxidant is ambient air. PEMFC systems have emerged as a possible replacement for internal combustion engines due to their efficiency, zero emission potential, and use of renewable fuels. Those used in transportation applications will experience unpredictable and widely varying power demand changes just like internal combustion engines in the majority of present vehicles. However, PEMFC systems are not currently cost effective; increasing their potential power density can improve their attractiveness. Moreover, hydrogen gas has a low density compared to liquid fuels, and even when pressurized can consume a significant volume. Thus it is advantageous to minimize the amount required for acceptable vehicle range. A simple way to accomplish these goals is to operate the PEMFC at its maximum allowed temperature. This has the effect of shifting the polarization curve upward; the reaction produces more power than at a lower temperature and requires no additional fuel or oxidant [1].

Previous authors [2–4] have assumed that a controller is available to perfectly maintain the fuel cell at its operating temperature. Unfortunately, the fuel cell cooling management work to date has been focused on modeling rather than control [5, 6]. There has been past work in internal combustion engine thermal management [7] and heat exchanger [8] control. Engine thermal management methods may be applied but require modification since: a fuel cell cooling system has less actuators; nearly all of the fuel cell waste heat must be rejected by the cooling system unlike an engine which rejects most of its waste heat with exhaust; there is a smaller temperature difference between the powerplant and surroundings which makes heat rejection more difficult; and the fuel cell power output and working life are greatly influenced by its operating temperature so its precise control is imperative. Next, the heat exchanger control was developed with the assumption that the fluid to be cooled is maintained at a constant mass flow rate. This approach will waste valuable fuel cell power. Thus, it is of primary interest to develop a fuel cell cooling system controller and validate the assumption that the fuel cell temperature can be maintained without large excursions when subject to fuel cell output power changes and other disturbances.

The objective of the work presented here is to develop a linear controller (or series of them) that can regulate the coolant and cooling air mass flow rates in an effort to ensure that the fuel cell internal temperature is maintained at a set value in the presence of noise and disturbance. Also, it is desired to find a set of μ-synthesis weighting functions, dependent only upon the linearization point, which can always give a suitable controller. The use of a general form speeds series controller construction since it becomes only a matter of application. Furthermore, performance of the resulting controllers is evaluated with simulation.

MODEL DEVELOPMENT

A complete modern fuel cell system model intended for transportation applications has previously been developed and simulated by Meyer and Yao [9]. The complete model is composed of four submodels: anode control volume, cathode control volume, fuel cell body, and cooling system. The cooling system referred to in this work combines the previous cooling system submodel and a modified fuel cell body submodel. They are joined together since it is desired to regulate the body temperature with the cooling system actuators. The states T_{fc}, $T_{clt,fc}$, $T_{clt,hex}$, $T_{ha,hex}$, and T_{hex} make up this new system. Their relationship is shown in Figure 1. The original fuel cell body submodel is the T_{fc} state nonlinear equation. States other than those listed here appear in it and their effect is lumped together in a disturbance term, $d_{T_{fc}}$. Sensor dynamics are not included since it is assumed that thin wire thermocouples are used; they can have a bandwidth over 300 rad/s [10]. The cooling system is in nonlinear state space form. To eventually apply μ-synthesis controller design it must be linearized. The linearized state space formulation models the response about an operating point:

$$\delta\dot{x} = A\delta x + B\delta u + B_d d_{T_{fc}} \tag{1}$$

$$\delta y = C\delta x \tag{2}$$

where:

$$\delta x = [\delta T_{fc} \;\; \delta T_{clt,fc} \;\; \delta T_{clt,hex} \;\; \delta T_{ha,hex} \;\; \delta T_{hex}]^T \tag{3}$$

$$\delta u = [\delta \dot{m}_{clt} \;\; \delta \dot{m}_{ha,hex}]^T \tag{4}$$

$$\delta y = \delta T_{fc} \tag{5}$$

$$B_d = [(m_{fc} c_{v,fc})^{-1} \; 0 \; 0 \; 0 \; 0]^T \tag{6}$$

$$C = \begin{bmatrix} 1 & 0 & 0 & 0 & 0 \end{bmatrix} \tag{7}$$

State matrices A and B are found from the linearized equations evaluated at a steady state operating condition. The non-

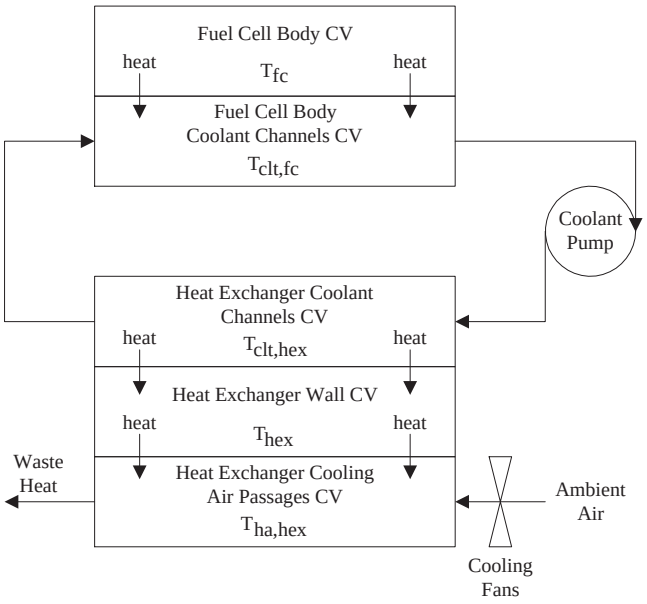

Figure 1. COOLING SYSTEM STATE RELATIONS

linear equations that they are derived from are found in [9]. The complete fuel cell system nonlinear model at steady state can be solved optimally to minimize the sum of the pump and fan output mass flow rates. This method is required because the pump and fan control efforts solution is not unique. The optimal solution requires the following inputs: desired fuel cell body temperature; anode pressure; oxidant stoichiometry ratio; and current density. It is assumed that the body temperature is also the value that the cooling control system should maintain. This then leaves current density as the only free parameter expected to vary. It is not unreasonable to hold the oxidant stoichiometry ratio constant and anode pressure constant when the system has a low pressure oxidant supply. Therefore, the operating point to linearize about is chosen to be the steady state values at the midpoint of a current density range of interest.

Nearly half of the terms of A and all those of B will change with the choice of a linearization point. Therefore, parameter uncertainty will be used to represent the expected variations of the linearized nonlinear terms in a range of operation. Each term's maximum and minimum parameter uncertainty is the upper and lower bound found in a current density range. The current density range is subdivided into 20 discrete points for finding these bounds at points other than the range endpoints. Remaining terms are kept at their nominal value.

The disturbance term, $d_{T_{fc}}$, is developed next. Fuel cell system optimal steady state solution values are used to compute the greatest disturbance magnitude in the current density range. The current density range is again subdivided into 20 discrete points. At each of these points the disturbance is evaluated with the current states and necessary terms from the linearized fuel cell body equation. The original nonlinear fuel cell body equation is not used directly since it is very difficult to separate out the effects of T_{fc} and the states not considered here. The maximum $d_{T_{fc}}$ is then referenced back to the original linearization point so that it is a state-like difference.

CONTROLLER DEVELOPMENT

μ-synthesis controller design is performed via D-K iteration. Detailed treatments can be found in [11–13]. μ-synthesis is well suited to the cooling system plant since it can create a linear controller that maintains robust performance in the presence of parameter and multiplicative input uncertainties. Robust performance means keeping the infinity norm of the weighted uncertain plant below one at all frequencies. This also gives closed loop robust stability; however, nominal stability must be checked separately. Parameter uncertainties contain the expected variations of the linearized nonlinear terms over a specified range of operation. Furthermore, one controller may not be able to satisfy the robust performance criteria over the entire current density with the weighting functions developed. Therefore, linear controllers may be designed for specific current density segments in which μ-synthesis leads to a robustly performing closed loop. Naturally, the resulting controllers would be scheduled with the present current density operating point.

Figure 2 shows the weighted uncertain design plant used. Table 1 defines the various inputs and outputs pictured. The uncertain plant, P_{unc}, contains both an augmented nominal plant which allows parameter uncertainties to be pulled out and weighted plant actuator input uncertainties. Each actuator input has an uncertainty weighting function. A typical uncertainty weighting is less than 10% at steady state while increasing to 200% at higher frequencies [11]. In this instance, error is assumed to be initially 5%, rising to 200%. The crossover frequency for the weights is chosen to be 20 rad/s. This corresponds to the first order response minimum break frequency of the linearized fan actuator dynamics found over the entire working range. For simplicity, both actuator input channels are assumed to have the same multiplicative uncertainty weighting function. This may be viewed as a conservative choice for the pump input channel. The resulting transfer function matrix is:

$$W_{mu} = \begin{bmatrix} \frac{2s+1.734}{s+34.68} & 0 \\ 0 & \frac{2s+1.734}{s+34.68} \end{bmatrix} \tag{8}$$

The remaining weighting functions are developed through system knowledge and performance guided iteration. Their general form is not specific to any current density range. W_{dist} is the disturbance weighting function which scales the normalized input disturbance d_1 up to the maximum expected value and shapes

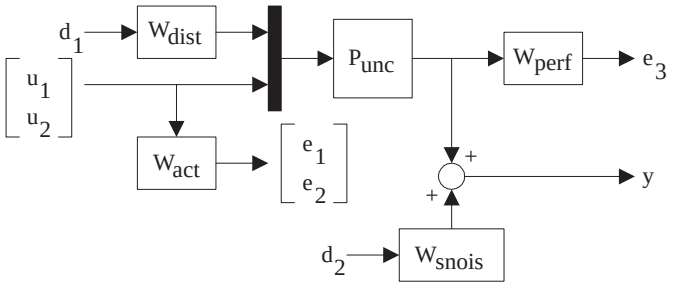

Figure 2. WEIGHTED UNCERTAIN DESIGN PLANT

Table 1. μ-SYNTHESIS DESIGN PLANT INPUTS AND OUTPUTS

Parameter	Definition
d_1	Normalized $d_{T_{fc}}$
d_2	Normalized d_{snois}
u_1	$\delta\dot{m}_{clt}$ Command
u_2	$\delta\dot{m}_{ha,hex}$ Command
e_1	Weighted Pump Control Signal
e_2	Weighted Fan Control Signal
e_3	Weighted δT_{fc}
y	δT_{fc}+Sensor Noise

its frequency content. A driver that tries to match the speed of other vehicles in traffic will typically have a velocity command to vehicle response closed loop bandwidth between 0.21 and 0.37 rad/s [14]. Furthermore, it is not unreasonable to expect step-like throttle changes as well. Thus, the disturbance scaling is passed through a 1 rad/s low pass filter. By giving the weighting function this structure, the resulting controller should be able to reject disturbances at the expected lower frequencies.

$$W_{dist} = \frac{d_{T_{fc},max}}{s+1} \tag{9}$$

The noise weighting function is determined from the expected interference caused by the cooling system flow devices. Brushless DC systems can produce noise at a devices rotational speed; thus noise may only occur between the minimum and maximum flow device speeds expected over the entire current density range. $\omega_{pmp,min}$ and $\omega_{pmp,max}$ are 13.7 and 822.9 rad/s, respectively. $\omega_{fan,min}$ is 3.7 rad/s and $\omega_{fan,max}$ is 593.2 rad/s. Therefore, noise can usually be expected between 3.7 and 822.9 rad/s. However, to attenuate potential higher frequency disturbances the weighting function will not roll off at the maximum frequency. Also, the maximum T_{fc} variation is considered to be constant throughout the noise frequency range. The magnitude of T_{fc} variation here is thought to be reasonable but not based on a specific experimental setup. Furthermore, a safety factor is included in the hope that it will lead to better sensor noise rejection by the resulting controller. The weighting function acts as a high pass filter with an initial 40 dB/decade rise before reaching 3.7 rad/s. The choice of this slope indicates that sensor noise is expected to rise rather suddenly before reaching its final constant value.

$$W_{snois} = \frac{f_S \Delta T_{fc}(\alpha s)^2}{(\alpha s+1)^2} \tag{10}$$

where:

$$\alpha = (\min\{\omega_{pmp,min}, \omega_{fan,max}\})^{-1} \tag{11}$$

$$f_S = 2 \tag{12}$$

$$\Delta T_{fc} = 0.5\ K \tag{13}$$

Up to this point, the emphasis has been on input weighting functions, however the output weighting functions are also needed to shape a resulting controller. W_{act} penalizes the use of control actuation. The fuel cell cooling system has two types of flow devices: coolant pump and heat exchanger cooling fans. The weighting functions penalize saturation as well as frequencies to avoid. The amount of remaining control actuation is found by subtracting the minimum in a current density segment from the overall maximum. Also, the actuator bandwidth is set between the disturbance and sensor noise break frequencies; it is chosen to be 2 rad/s. This should allow sufficient disturbance response as well as sensor noise attenuation. Bandwidth could have been chosen larger for both actuators. Linearization of flow device dynamics in [9] suggest that the coolant pump has a first order response maximum time constant of 300^{-1} s while the cooling fan value is 20^{-1} s. Each time constant is the maximum in the entire operating range. Unfortunately, use of these values would have conflicted with the need to attenuate the sensor noise. Also, a very fast negative pole is included to make each weighting function proper and stable.

$$W_{act,pmp} = \frac{s+\omega_{act,bw}(\Delta\dot{m}_{clt,cds})^{-1}}{1\cdot 10^{-6}s+\omega_{act,bw}} \tag{14}$$

$$W_{act,fan} = \frac{s+\omega_{act,bw}(\Delta\dot{m}_{ha,hex,cds})^{-1}}{1\cdot 10^{-6}s+\omega_{act,bw}} \tag{15}$$

where:

$$\Delta\dot{m}_{cds} = \dot{m}_{max} - \dot{m}_{min,cds} \tag{16}$$

$$W_{act} = \begin{bmatrix} W_{act,pmp} & 0 \\ 0 & W_{act,fan} \end{bmatrix} \tag{17}$$

Finally, W_{perf} is used to drive the performance variable to its desired value. Recall that the desired fuel cell body temperature is one of the operating point values that the system is linearized about. Therefore, the weighting function penalizes deviations of δT_{fc} from zero with a pseudo-integrator weighting function [12]. More penalty is placed on deviation at lower frequencies for better step disturbance attenuation.

$$W_{perf} = \frac{1/12}{s+\varepsilon} \tag{18}$$

ε is a small number so that the weighting function approximates a pure integrator. A value of 0.01 is found to work here.

RESULTS

The maximum allowable mass flow rates of the coolant and cooling air are chosen as 5 and 10 kg/s, respectively. These are approximately 25% more than the expected fuel cell system steady state optimal solution values at the maximum fuel cell power peak current density of 1.5 A/cm^2. This is the same solution method described earlier which minimizes the total cooling system effort. Choosing the maximum mass flow rates to be greater than their expected steady state values leaves some control authority for quick transient response. It is desired to control the fuel cell body temperature so that it remains at 367 K during operation. This temperature can only be reached when the fuel cell is operating above 0.24 A/cm^2. Therefore, the current density range is [0.24,1.5] A/cm^2. The range is covered by a minimum of seven controllers designed using the weighting functions presented. The current density segments and needed weighting function values are listed in Tbl. 2. The segments were identified by iteratively adjusting them until the resulting controller ensured a peak structured singular value μ upper bound less then one over all frequencies. The μ-synthesis controllers have full order of at least 31. A comparison of Hankel singular values led to a reduction to order eight for all. Each reduced order controller and associated nominal plant is closed loop stable.

The linear controllers are applied to the whole fuel cell system nonlinear model developed in [9]. The most recent current density value is used to select an appropriate cooling system controller. All control inputs other than the coolant and cooling air mass flow rates that the nonlinear model requires are simply set

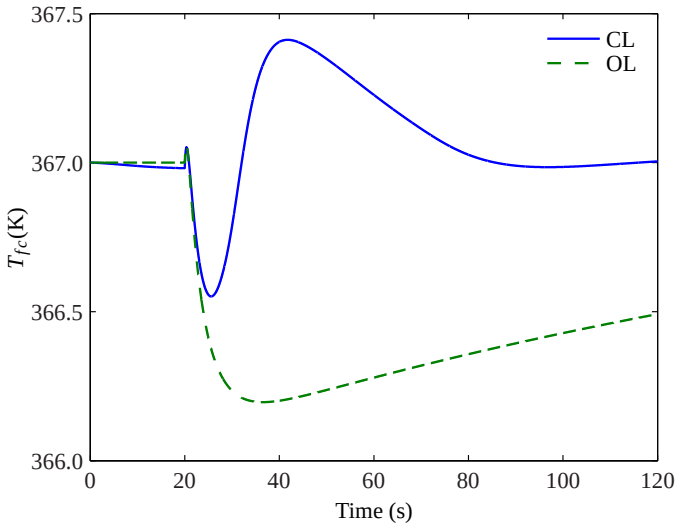

Figure 3. T_{fc} RESPONSE FROM 0.25 TO 1.5 A/cm^2 STEP

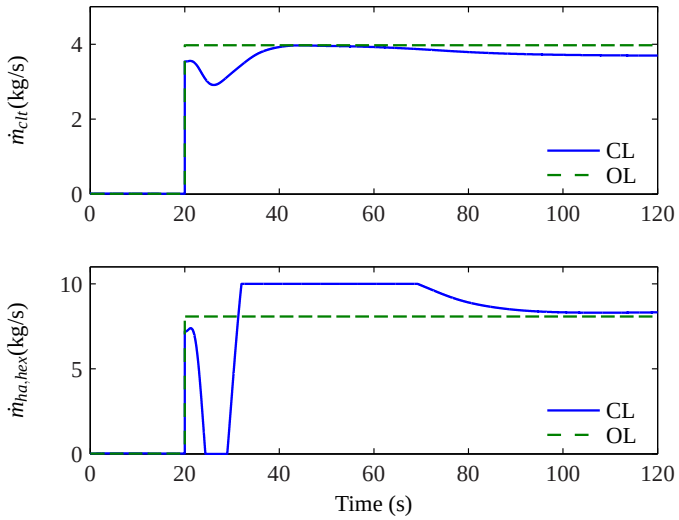

Figure 4. ACTUATOR RESPONSE FROM 0.25 TO 1.5 A/cm^2 STEP

to their expected steady state optimal solution values at a specific operating point. Noise is generated at the lowest frequencies that the pump and cooling fan can be expected to be operating at in the present current density segment. The noise magnitude contributed by each is assumed to be 0.25 K so that the total cannot ever exceed 0.5 K.

Three simulations are carried out to show system performance. The first is a step change from 0.25 to 1.5 A/cm^2 after 20 s to show response during a severe change in current density. The next is also a step; current density changes from 0.25 to 0.875 A/cm^2 at 20 s. This is half the current density change

Table 2. μ-SYNTHESIS DESIGN DATA

Parameter	1	2	3	4	5	6	7
Current Density(A/cm^2)	[0.24,0.27)	[0.27,0.45)	[0.45,0.93)	[0.93,1.18)	[1.18,1.34)	[1.34,1.44)	[1.44,1.50]
$d_{T_{fc},max}$(W)	$4.53{\cdot}10^2$	$3.97{\cdot}10^3$	$2.15{\cdot}10^4$	$1.67{\cdot}10^4$	$1.33{\cdot}10^4$	$9.46{\cdot}10^3$	$6.14{\cdot}10^3$
$\Delta\dot{m}_{clt,cds}$(kg/s)	5.00	4.98	4.85	4.23	3.54	2.71	1.83
$\Delta\dot{m}_{ha,hex,cds}$(kg/s)	10.00	9.96	9.69	8.43	7.02	5.33	3.54

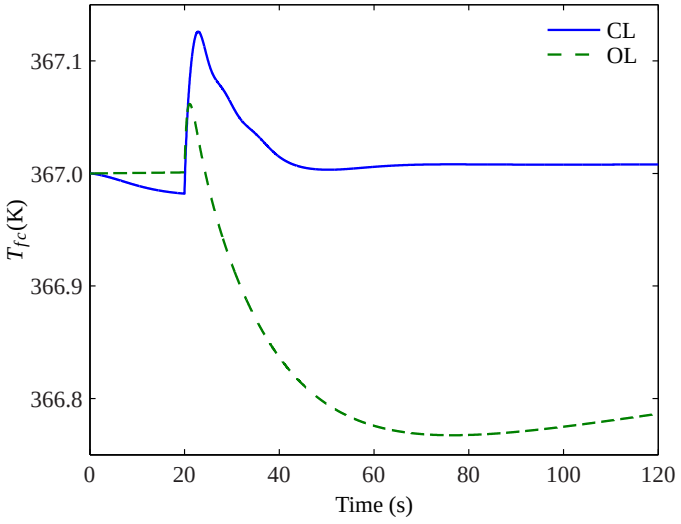

Figure 5. T_{fc} RESPONSE FROM 0.25 TO 0.875 A/cm^2 STEP

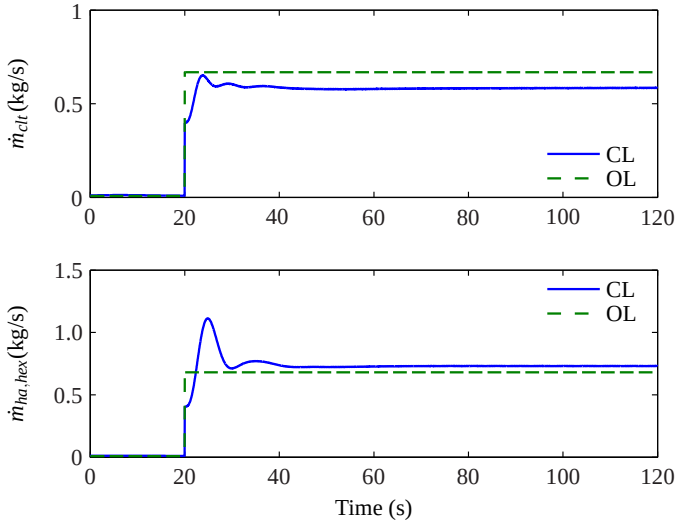

Figure 6. ACTUATOR RESPONSE FROM 0.25 TO 0.875 A/cm^2 STEP

of the first step. The step input simulations are both 120 s long. The controller performance is also compared to simple open loop control in these simulations. Open loop control is used also since the fuel cell has a large thermal capacitance which should damp the severity of the body temperature response. Coolant and cooling air mass flow rates set by the expected optimal steady state values may also produce sufficient transient performance. Finally, to show closed loop sinusoid disturbance rejection, current density is allowed to vary from 0.25 to 1.5 A/cm^2 with a period of 0.4 rad/s for 60 s. The maximum flow rates are saturation limited and nonnegative in each.

Figures 3-4 display the fuel cell temperature and coolant system actuator reactions during the 0.25 to 1.5 A/cm^2 step, respectively. Both the closed loop response (with the controllers developed here) and an open loop response (using the coolant and air flow rates from the optimal steady state solution) are shown. The closed loop temperature response shows a maximum drop of 0.4 K while the open loop response falls 0.8 K. Meanwhile, the closed loop system has a 0.4 K overshoot. At the end of the simulation, the closed loop system has recovered while the open loop one is still 0.5 K below desired. It is also interesting that both the closed and open loop show a quick temperature rise of approximately 0.1 K at the step change before it falls off. This is mostly due to cooling system response dynamics but the oxidant supply dynamics also have an effect. They are part of the overall fuel cell model and are not detailed here. The oxidant supply dynamics produce a small but noticeable lag into oxidant delivery. Thus, the cathode exhaust does not carry away as much waste heat as it will after the lag. Next, actuator response of both the open loop and closed loop systems can be compared. Obviously, the open loop response has no undershoot or overshoot since it just changes along with the step. The coolant pump has a similar response to the open loop response. However, the cooling fans rise, shut down, and then saturate for approximately 30 s. At the end of the simulation the closed loop and open loop actuators have slightly different values. This is due to the realization that the open loop values are from an optimization solution while the closed loop values are driven by the controller. The open loop coolant and cooling air mass flow rates required to maintain the fuel cell body temperature do not have a unique solution in the

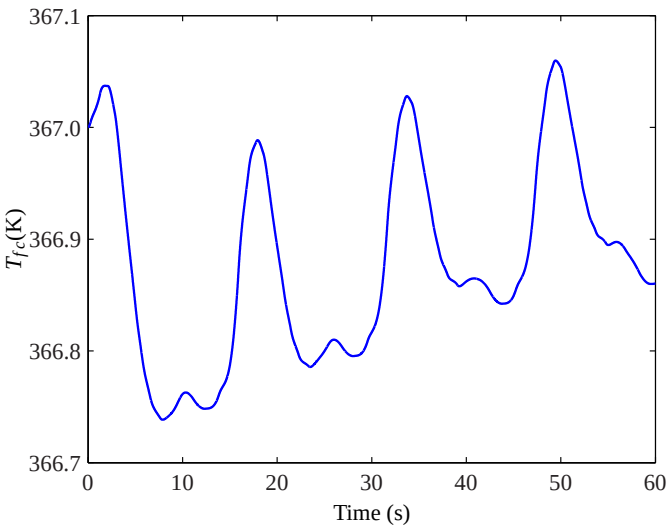

Figure 7. T_{fc} RESPONSE FROM 0.25 TO 1.5 A/cm^2 SINUSOID

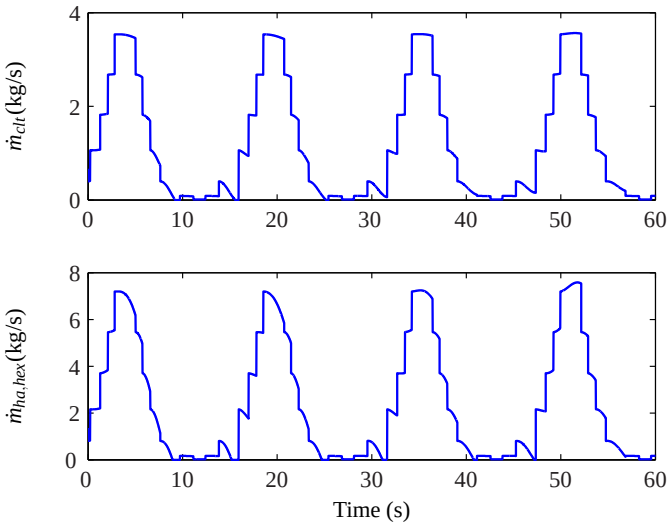

Figure 8. ACTUATOR RESPONSE FROM 0.25 TO 1.5 A/cm^2 SINUSOID

current problem formulation. The coolant mass flow rates differ by approximately 0.3 kg/s while the cooling air varies a little more than 0.2 kg/s. Neither closed loop actuator response shows the effects of the sensor noise. This simulation seems to show that the closed loop controllers do not offer much advantage over simple open loop control. However, the open loop actuator values are based upon perfect knowledge of the plant. In reality, it is very unlikely that the open loop response would appear as good since it has no feedback mechanism that can handle parameter or model structure uncertainties.

The second, smaller step reaction is shown in Figs. 5-6. The closed loop and open loop response are both shown again for comparison. Closed loop T_{fc} response begins to drift even before the step input at 20 s. This phenomenon is also present in the previous step results, though not as readily apparent with the y-axis scale used. To start the simulation, the closed loop response is seeded with open loop initial actuator values. It is expected that the actuator values will then be updated in the closed loop. The controllers do not add integrators to the closed loop response, thus a small amount of error is not unreasonable. This step simulation has the same general trends that were seen with the previous step input. Open loop temperature response shows a maximum drop of 0.24 K and only recovers to within 0.21 K at the end of the simulation. Meanwhile, the closed loop response has almost no undershoot after the step and only overshoots the desired temperature by 0.13 K. It also is able to recover to within 0.008 K in approximately 20 s. Also, a small open loop body temperature spike of 0.06 K occurs at the beginning of the step change. The same reasoning from the previous results is also applicable to this. However, the continued increase of body temperature seen in the closed loop after the step change is most likely due to the controller response. Actuator response is also similar to that of the first simulation. The closed loop and open loop actuator final simulation values are different again. The coolant and cooling air mass flow rates differ by 0.08 and 0.10 kg/s, respectively. The same logic can be applied to explain this difference. The closed loop cooling fan actuation is much smoother than the previous simulation. It still has an overshoot of approximately 50% of final simulation value, but at least it does not saturate. Finally, both actuator responses in the closed loop simulation show controller rejection of the sensor noise.

With the designed controllers, the closed loop cooling system should attenuate disturbances up to 1 rad/s. Figures 7-8 are the respective temperature and actuator responses to a sinusoid current density disturbance from 0.25 to 1.5 A/cm^{2}with a period of 0.4 rad/s. Only closed loop results are shown. The four large body temperature peaks at approximately 2, 18, 34 and 50 s lead operation at 1.5 A/cm^2 by roughly 2 s. The smaller peaks at approximately 10, 26, 42, and 58 s lead the 0.25 A/cm^2 disturbance by about 2 s also. The body temperature response shows only a maximum 0.26 K drop and 0.06 K rise from desired during the simulation. The controllers do not completely reject the disturbance but are able to attenuate it. Moreover, it can be readily seen that the desired actuator efforts progress through all of the different controllers. It is also apparent that the sensor noise is not impacting any controller in a meaningful way.

It is also possible to simulate the cooling system response from high to low current density. However, the results are not as interesting. Generally, the body temperature will initially fall a small amount,less than 0.4 K, and then begin to recover. Meanwhile, the flow devices go to zero and remain there until the body temperature nearly reaches its desired value.

CONCLUSIONS

A set of seven linear controllers has been successfully constructed with μ-synthesis and a linearized fuel cell cooling system. Parameter uncertainty has been used to capture linearized term variations that can occur at different evaluation points in a current density segment. It was found possible to design a common set of weighting functions that can be used within different current density range segments. These segments were then the only design parameter left for each controller. This greatly simplified the construction of an entire series of scheduled controllers. Also, the fuel cell body temperature showed at most 0.1% variation during closed loop simulation when subject to the most severe current density step changes. Open loop simulation showed 0.2% variation during the same test. However, even though open loop control gives similar results, near perfect plant knowledge is required. It is anticipated that the open loop control results will not be nearly so comparable in actual usage. The closed loop sinusoidal current density disturbance simulation results also show very little deviation from the desired body temperature. Therefore, it is not unreasonable to assume then that the body temperature is constant when cooling system closed loop control is active. The fuel cell body temperature dynamics will only need to be considered outside of the cooling system when it is inactive. Keeping the cooling system off below a certain threshold will increase the net power from the fuel cell since the coolant pump and cooling fans are parasitic devices. Finally, the coolant flow rate does not saturate during any of the simulations. It may be worthwhile to explore whether or not the pump size can be reduced. A reduction of the pump's maximum flow rate will most likely lower the cost and mass penalty associated with it. Unfortunately, it will also change the pump actuator weighting function and require the creation of a new set of controllers.

Future research should include the application of the designed controllers to an experimental setup to ensure they perform as well in actuality as in simulation. This will also let realistic comparisons to open loop control to be made.

ACKNOWLEDGMENT

Thanks go to the National Defense Science and Engineering Graduate Fellowship administered by the American Association of Engineering Education for supporting Richard Meyer.

REFERENCES

[1] Larminie, J., and Dicks, A., 2003. *Fuel Cell Systems Explained*, 2nd. ed. John Wiley & Sons Limited, West Sussex, England.

[2] Pukrushpan, J. T., Stefanopoulou, A. G., and Peng, H., 2004. *Control of Fuel Cell Power Systems: Principles, Modeling, Analysis and Feedback Design*, 1st. ed. Advances in Industrial Control. Springer-Verlag Limited, London, England.

[3] Pathapati, P., Xue, X., and Tang, J., 2005. "A New Dynamic Model for Predicting Transient Phenomena in a PEM Fuel Cell System". *Renewable Energy*, **30**(1), pp. 1 – 22.

[4] Xue, X., Tang, J., Smirnova, A., England, R., and Sammes, N., 2004. "System Level Lumped-Parameter Dynamic Modeling of PEM Fuel Cell". *Journal of Power Sources*, **133**(2), pp. 188 – 204.

[5] Zhang, Y., Ouyang, M., Lu, Q., Luo, J., and Li, X., 2004. "A Model Predicting Performance of Proton Exchange Membrane Fuel Cell Stack Thermal Systems". *Applied Thermal Engineering*, **24**(4), pp. 501 – 513.

[6] Zhang, Y., Ouyang, M., Jianxi, L., Zhao, Z., and Yongjun, W., 2003. "Mathematical Modeling of Vehicle Fuel Cell Power System Thermal Management". *SAE Paper 2003-01-1146*.

[7] Setlur, P., Wagner, J. R., Dawson, D. M., and Marotta, E., 2005. "An Advanced Engine Thermal Management System: Nonlinear Control and Test". *IEEE/ASME Transactions on Mechatronics*, **10**(2), pp. 210 – 220.

[8] Alvarez-Ramirez, J., Cervantes, I., and Femat, R., 1997. "Robust Controllers for a Heat Exchanger". *Industrial & Engineering Chemistry Research*, **36**(2), pp. 382 – 388.

[9] Meyer, R. T., and Yao, B., 2006. "Modeling and Simulation of a Modern PEM Fuel Cell System". *Proceedings of the 4th International Fuel Cell Science, Engineering and Technolgy Conference*(To Be Presented).

[10] Omega Engineering, Inc., 2006. Thermocouple Tutorial. URL `http://www.omega.com/thermocouples.html`.

[11] Skogestad, S., and Postlethwaite, I., 1996. *Multivariable Feedback Control: Analysis and Design*, 1st. ed. John Wiley & Sons, West Sussex, England.

[12] Zhou, K., and Doyle, J. C., 1998. *Essentials of Robust Control*, 1st. ed. Prentice-Hall, New Jersey, USA.

[13] Balas, G., Chiang, R., Packard, A., and Safonov, M., 2005. *Robust Control Toolbox User's Guide: Version 3*, 3rd. ed. MathWorks, Massachusetts, USA.

[14] Allen, R. W., Magdaleno, R. E., Serafin, C., Eckert, S., and Sieja, T., 1997. "Driver Car Following Behavior Under Test Track and Open Road Driving Condition". *SAE Paper 970170*.